ARCHIVES OF MECHANICS
Arch. Mech. **72** (4), 307–321, 2020, DOI: 10.24423/aom.3498

A new dynamic model for a rotating beam carrying extra partially distributed mass

A. ALTINKAYNAK*), M. GÜRGÖZE

*Mechanical Engineering Department, Istanbul Technical University, Gümüşuyu, 34437, Istanbul, Turkey, *)e-mail: altinkayna@itu.edu.tr (corresponding author)*

In this paper, a new dynamic model for the vibration analysis of an inward-oriented rotating cantilever beam with extra distributed mass was presented. The derived differential equation of motion was solved using the meshless methods of generalized Multiquadric Radial Basis Function (RBF) and the eigenfrequencies of the system were determined. The same problem was also modeled using the finite element method and the results were compared to validate the accuracy of the proposed model. Later, the effect of the partially distributed mass amount and location on the eigenfrequencies was studied for various beam lengths. The results showed that the eigenfrequency at a constant rotational speed mostly decreased unless the mass was located at the free end of the beam. The location of the mass had a greater effect on the first eigenfrequency compared to the second and third eigenfrequencies. A joint dimensionless eigenfrequency was found at a specific rotational speed regardless of the distributed mass. Nearly constant dimensionless eigenfrequencies could be obtained for a wide range of rotational speeds by adjusting the distributed mass.

Key words: mechanical vibrations, modal analysis, rotating cantilever beam, partially distributed mass, radial basis functions-based meshless method.

1. Introduction

The dynamic response of a system has a critical importance in the design of structures attached to rotating frames. In many practical engineering applications such as rotor blades in helicopters, centrifugal applications, wind turbines, and satellites, the dynamic response of the system has to be determined accurately in order to achieve a reliable operation and economically feasible design. Due to this reason, the dynamic characteristics of rotating structures have been reported in the literature. The bending vibration of a rotating beam was investigated by Schilhansl [1]. The linear differential equation of motion was derived and the natural frequencies of the beam system were obtained. Further studies included the effect of variation on the cross-sectional shape and bending rigidity [2], hub radius [2, 3], different external forces such as tip mass [2, 4] and elastic foundation [5] on the dynamic behavior of rotating beams. The nonlinear effects due to geometry and dynamics of the rotating beams were also studied.

Another group of studies focused on the non-linear effect of Coriolis forces [6, 7], curvature [8, 9], axial strain [10], and stretch deformation [11] on the modal characteristics of rotating beams.

The dynamic behavior of inward-oriented rotating beams had a special attention because rotation-induced compressive stresses may cause instability due to buckling. For these systems, the critical rotational speeds for buckling were obtained by [12–14]. Numerical instabilities were observed for a small ratio of rigid ring radius to beam length (α) [12, 13]. The limiting value of α for eliminating in-plane buckling were also studied [15, 16]. Other efforts focused on determining the eigenfrequencies of the inward-oriented rotating beams for a variety of α and it was found that the characteristics of the eigenfrequencies depended on α and rotational speed Ω [17–19].

Various numerical approaches were used to determine the modal characteristics of rotating beam systems. Some of the numerical methods implemented were Ritz method [1], integrating matrix procedure [15], finite element method [3, 11], perturbation approach [9, 13, 17], Galerkin's method [14, 19], and the Frobenius method [2]. Researchers have been seeking a stable and accurate numerical algorithm that can be implemented to determine the modal characteristics of rotating beam systems. Recently, Gunda and Ganguli [20] have proposed stiff-string basis functions used with the finite element method for faster convergence of rotating beam problems. To improve convergence behavior in rotating beam problems, another basis function with collocation points was developed for the finite element method [21] where the behavior of the basis functions depends on the rotational speed, the location of an element, and the collocation points. Closed form solutions of a rotating beam were found using an inverse problem approach [22] in which separate polynomial shape functions were assumed for individual modes. Panchore *et al.* [23, 24] implemented the meshless local Petrov–Galerkin method to solve the weak form of the rotating beam problems. This method eliminates the need for a mesh to construct the shape function. However, it requires an integration step which is not a straightforward process in meshless methods due to a lack of mesh that determines the integration domain. The strong form solution of the problem eliminates the need of integration. Yet, to the authors' knowledge, the strong form of the rotating beam problems has not been investigated using meshless methods.

Even though the finite element method has been used extensively in modal analysis of rotating beams, the analysis requires two-step procedure to include the effect of the centrifugal forces on the eigenfrequencies [25]. First, a stationary analysis is performed to determine the stationary deformation due to centrifugal forces. Then, the results are used as a linearization point for the modal analysis. Thus, the modal analysis depends on the successful completion of the stationary analysis which may not be the case especially at high speeds.

In this study, a new dynamic model to investigate the vibration characteristics of an inward-oriented rotating beam carrying extra partially distributed mass was proposed. The differential equation of motion characterizing the beam system was derived using Hamilton's principle. An efficient and accurate radial basis function (RBF) collocation method was implemented to determine the eigenfrequencies by solving the strong form of the differential equation. The effect of the partially distributed mass on the eigenfrequencies was studied when the mass was located towards the free end, middle and clamped end of the beam. The characteristics of eigenfrequencies were also analyzed for various beam lengths.

2. Derivation of the differential equation of motion

Figure 1 shows the rotating beam system with partially distributed mass. The system includes an elastic beam with a total length of L clamped onto a rigid ring with a radius of R. The other end of the elastic beam is free and the Euler–Bernoulli beam theory was used to model the elastic beam. The rigid ring is rotating at a constant angular speed (Ω) around a perpendicular axis passing through its center. The bending rigidity of the beam is given as EI The mass per unit length of the beam is defined along its axis with a function $\mu(\xi)$ which is equal to:

$$\mu(\xi) = \mu + \{H(\xi - L_1) - H(\xi - (L_1 + L_2))\}\mu_2 \tag{2.1}$$

where H is the Heaviside unit step function, μ and μ_2 are the mass per unit length of the elastic beam and partially distributed mass, respectively, ξ is the

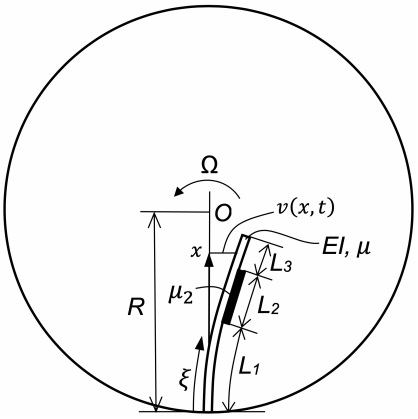

FIG. 1. An inward-oriented elastic beam carrying partially distributed mass attached to a rotating rigid ring.

spatial coordinate for the partially distributed mass, L_1 is the distance of partially distributed mass to the clamped end of the beam and L_2 is the length of the partially distributed mass as shown in Fig. 1. It was assumed that the partially distributed mass per unit length (μ_2) shown in Fig. 1 has no bending rigidity. This condition may be observed in rotating systems when there is soot deposition.

From Hamilton's principle, the governing differential equation of motion for an inward-oriented rotating beam with proper boundary conditions can be written as [17]:

$$\begin{aligned} &EIv''''(x,t)+\mu(\xi)\ddot{v}(x,t)-\mu(\xi)\Omega^2 v(x,t)+\mu(\xi)\Omega^2\{F_a(x)v'(x,t)\}'=0,\\ &v(0,t)=v'(0,t)=v''(L,t)=v'''(L,t)=0 \end{aligned} \tag{2.2}$$

where $v(xt)$ is the beam deflection and the axial force acting on the beam due to the centrifugal force $F_a(x)$ is defined as:

$$F_a(x)=\int_x^L \mu(\xi)\Omega^2(R-\xi)\,d\xi. \tag{2.3}$$

To determine the axial force $F_a(x)$ acting on the beam section x because of the centrifugal force, the beam was considered having three separate regions as shown in Fig. 1. $F_a(x)$ for each section was calculated by integrating Eq. (2.3). The results of these integrations are given in Eq. (2.4)

$$\begin{aligned} F_{a1}(x)&=\mu\Omega^2\left\{\left[R(L-x)-\frac{1}{2}(L^2-x^2)\right]\right.\\ &\qquad\left.+\frac{\mu_2}{\mu}\left[RL_2-L_1L_2-\frac{L_2^2}{2}\right]\right\},\quad 0\le x\le L_1,\\ F_{a2}(x)&=\mu\Omega^2\left\{\left[R(L-x)-\frac{1}{2}(L^2-x^2)\right]\right.\\ &\qquad\left.+\frac{\mu_2}{\mu}\left[R(L_1+L_2-x)-\frac{1}{2}\left[(L_1+L_2)^2-x^2\right]\right]\right\},\quad L_1\le x\le L_1+L_2,\\ F_{a3}(x)&=\mu\Omega^2\left[R(L-x)-\frac{1}{2}(L^2-x^2)\right],\quad L_1+L_2\le x\le L. \end{aligned} \tag{2.4}$$

Assuming the solution follows a harmonic behavior in the form of

$$v(x,t)=y(x)\cos(\omega_i t),$$

partial differential equation given in Eq. (2.2) leads to the dimensionless form of the following ordinary differential equation systems and the corresponding

boundary conditions:

$$
\begin{aligned}
&y_1''''(\bar{x}) + \bar{\Omega}^2[\alpha_\mu \bar{b_1} - f(\bar{x},\alpha)]y_1''(\bar{x}) \\
&\qquad - \bar{\Omega}^2 f'(\bar{x},\alpha)y_1'(\bar{x}) - \bar{\Omega}^2 y_1(\bar{x}) = \lambda_i y_1, \quad 0 \le \bar{x} \le \alpha_1, \\
&y_2''''(\bar{x}) + \bar{\Omega}^2[\alpha_\mu \bar{b_2}(\bar{x}) - f(\bar{x},\alpha)]y_2''(\bar{x}) + \bar{\Omega}^2[\alpha_\mu \bar{b_2}'(\bar{x}) - f'(\bar{x},\alpha)]y_2'(\bar{x}) \\
&\qquad - (1+\alpha_\mu)\bar{\Omega}^2 y_2(\bar{x}) = (1+\alpha_\mu)\lambda_i y_2, \quad \alpha_1 \le \bar{x} \le \alpha_2, \\
&y_3''''(\bar{x}) - \bar{\Omega}^2 f(\bar{x},\alpha)y_3''(\bar{x}) - \bar{\Omega}^2 f'(\bar{x},\alpha)y_3'(\bar{x}) - \bar{\Omega}^2 y_3(\bar{x}) = \lambda_i y_3, \quad \alpha_2 \le \bar{x} \le 1,
\end{aligned}
$$

$$
\begin{aligned}
&y_1(0) = 0, \quad y_1(\alpha_1) = y_2(\alpha_1), \quad y_2(\alpha_2) = y_3(\alpha_2), \quad y_3''(1) = 0, \\
&y_1'(0) = 0, \quad y_1'(\alpha_1) = y_2'(\alpha_1), \quad y_2'(\alpha_2) = y_3'(\alpha_2), \quad y_3'''(1) = 0, \\
&\qquad\quad y_1''(\alpha_1) = y_2''(\alpha_1), \quad y_2''(\alpha_2) = y_3''(\alpha_2), \\
&\qquad\quad y_1'''(\alpha_1) = y_2'''(\alpha_1), \quad y_2'''(\alpha_2) = y_3'''(\alpha_2),
\end{aligned} \tag{2.5}
$$

where dimensionless parameters are defined as:

$$
\begin{aligned}
&\bar{x} = \frac{x}{L}, \quad \omega_0^2 = \frac{EI}{\mu L^4}, \quad \bar{\Omega} = \frac{\Omega}{\omega_0}, \quad \lambda_i = \frac{\omega_i^2}{\omega_0^2}, \\
&\alpha_\mu = \frac{\mu_2}{\mu}, \quad \alpha_1 = \frac{L_1}{L}, \quad \alpha_2 = \frac{L_1 + L_2}{L}, \quad \alpha = \frac{R}{L}, \\
&f(\bar{x},\alpha) = (1-\bar{x})\left[\frac{1}{2}(1+\bar{x}) - \alpha\right], \\
&\bar{b_2}(\bar{x}) = \alpha(\alpha_2 - \bar{x}) - \frac{1}{2}(\alpha_2^2 - \bar{x}^2), \\
&b_1 = \frac{RL_2}{L^2} - \frac{L_1 L_2}{L^2} - \frac{L_2^2}{2L^2},
\end{aligned} \tag{2.6}
$$

ω_i are the eigenfrequencies of the rotating beam on the rigid ring plane. The equations given in Eq. (2.5) that formulate the beam system shown in Fig. 1 were used to complete the modal analysis. If interested in the outward-oriented rotating beam system, the solution can be obtained by selecting $\alpha < 0$. In the derivation of equations given in Eq. (2.5), it was also assumed that the partially distributed mass has no bending rigidity. When partially distributed mass has a constant bending rigidity, this can be accounted for by introducing a coefficient in Eq. (2.5) at the interval $\alpha_1 \le \bar{x} \le \alpha_2$.

3. Numerical method

The eigenfrequencies of the rotating beam system described in Eq. (2.5) were determined using the radial basis function (RBF) collocation method. The RBF

collocation method is a meshless method that eliminates the need for mesh generation. KANSA [26, 27] implemented the RBF collocation method using multiquadric (MQ) RBFs to solve partial differential equations. Generalized MQ family of RBFs can be defined as in Eq. (3.1):

$$\phi(x) = (1 + (\varepsilon r)^2)^{\beta}, \qquad \varepsilon > 0, \beta \in \mathbb{R} \setminus \mathbb{N}_0 \tag{3.1}$$

where $r = x_i - x_j$ is the distance between the current domain point x_i and the center points x_j, ε is the shape parameter and β is the parameter that defines the type of the RBF. For $\beta < 0$ the functions are defined as the inverse multiquadric (IMQ) RBFs and for $\beta > 0$, MQ RBFs are obtained. Parameters ε and β affect the numerical stability and the solution of the partial differential equation. Points x_i may be located in the domain or at the boundaries, whereas the location of the center points x_j may also be outside of the domain. The approximation of the unknown function $y(x)$ at point x_i can be defined as the linear combination of RBFs which is written as:

$$y(x_i) = \sum_{j=1}^{N_c} c_j \phi_j(x_i), \qquad y'(x_i) = \sum_{j=1}^{N_c} c_j \phi_j'(x_i) \tag{3.2}$$

where N_c is the total number of center nodes and c_j are the constants to be determined. The derivatives of the unknown function given in Eq. (3.2) can be written as linear combinations of the RBF derivatives because c_j are constants. Substituting Eq. (3.2) into the differential equations and boundary conditions given in Eq. (2.5), the following collocation approximation is obtained:

$$\underbrace{\begin{bmatrix} L[y(x)] \\ B[y(x)] \end{bmatrix}}_{[A]} \{c\} = \{0\} \tag{3.3}$$

where L and B are the differential and boundary operators that define the differential equation and the boundary conditions given in Eq. (2.5), respectively. Equation (2.5) is reorganized to make the righthand side of the equation zero and the matrix form given in Eq. (3.3) was obtained. If the problem is well-posed, Eq. (3.3) has a unique solution and the coefficient vector $\{c\}$ can be determined. Equation (3.2) is then used to calculate the unknown variable field of y and its derivatives. However, our interest was to determine the eigenvalues λ_i that makes the determinant of matrix $[A]$ zero for non-trivial solutions. The critical rotational speeds for buckling were obtained if $\lambda = 0$. Eigenvalues are related to the eigenfrequencies (natural frequencies) of the system through the equation given in Eq. (2.6). The eigenmodes of the system can then be obtained using Eqs. (3.2) and (3.3) if needed.

Since the determinant is defined only for square matrices, $[A]$ has to be in the form of a square matrix for this problem. This requirement generates a limitation between the number of center nodes (N_c) and domain/boundary nodes. The number of domain nodes (N_d) and boundary conditions determine the row size whereas the number of center nodes determines the column size. For a total number of domain and boundary nodes of N_d and N_b, respectively, the total number of center nodes should be selected as $N_d + N_b$ to guarantee a square matrix. The total number of boundary nodes is $N_b = 4$ for the problem defined by Eq. (2.5) because two boundary conditions are imposed at each boundary.

It is known that the error on the boundaries tends to be larger than anywhere else in the domain in the RBF collocation method [28]. Due to this reason, FEDOSEYEV *et al.* [29] developed a method to impose not only the boundary conditions but also the partial differential equation at the boundary locations to reduce the error at the boundaries. This approach was followed in this study. The question of how the center nodes should be located is still an active area of research. Center nodes can be inside and/or outside of the domain or at the boundaries. In this study, center nodes for each boundary node were selected to be outside of the domain because it was found that selecting center nodes outside the domain generally give a smaller error values at the boundaries [30]. The distribution of domain, boundary and center nodes are given in Fig. 2. Center and domain nodes were uniformly distributed along the beam axis.

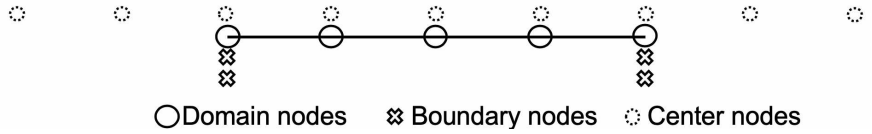

FIG. 2. The distribution of domain, boundary, and center nodes along the axis of the beam.

3.1. Determining the parameters of ε and β

Important parameters affecting the stability and the accuracy of the solution are the shape parameter ε, MQ parameter β, and the number of domain nodes N_d. As N_d increases, the relative error has a tendency to decrease. However, further increase in the number of domain points results in ill-conditioning of $[A]$. A mathematical representation of the error norm bound as a function of parameters ε and β has not been established yet for modal analysis problems. For this reason, a sensitivity analysis of ε, β and N_d was performed for the inward-oriented uniform cantilever beam with no extra added mass which has an available numerical solution [17]. In the sensitivity analysis, the variation of ε and β in the range of $0.1 \leq \varepsilon \leq 3$ and $-10 \leq \beta \leq 10$ was investigated and

the results were compared with the numerical results given in [17]. The results were obtained using the proposed meshless numerical scheme for three different rotational speeds with $\alpha = 0.5$. The absolute relative error was less than 1% in the range of $0.5 \leq \varepsilon \leq 2$ and $1 < \beta < 5$. In this range of ε and β, N_d was increased and the analysis was repeated. Once $N_d \geq 10$, numerical instabilities were observed in the solutions due to ill-conditioning. Due to this reason N_d was set to 9 and a combination of ε and β that minimized the absolute relative error was investigated in the range of $0.5 \leq \varepsilon \leq 2$ and $1 < \beta < 5$. A suitable combination was found as $\varepsilon = 0.75$ and $\beta = 1.35$ The comparison of the numerical results obtained from [17] and the proposed method is shown in Table 1. Good agreement between the results were observed especially at relatively small rotational speeds. As the rotational speed increased, the relative error on the eigenfrequencies tended to increase with a maximum of 0.8%. If needed, more accurate results at high rotational speeds could be obtained by increasing the number of domain nodes with local support [31]. The error levels less than 1% were considered as sufficient and the values of $N_d = 9$, $\varepsilon = 0.75$, and $\beta = 1.35$ were also used for the problem with extra partially distributed mass.

Table 1. First three dimensionless eigenfrequencies of the inward-oriented uniform cantilever beam attached to a rotating rigid ring with $\varepsilon = 0.75$, $\beta = 1.35$, and $N_d = 9$.

$\bar{\Omega}$	1.7580	11.0173	30.8486
$\sqrt{\bar{\lambda}_1}$	3.2446	NA	NA
$\sqrt{\bar{\lambda}_1}^{[17]}$	3.2454	NA	NA
Abs. relative error (%)	0.02	NA	NA
$\sqrt{\bar{\lambda}_2}$	22.1128	25.0435	39.4913
$\sqrt{\bar{\lambda}_2}^{[17]}$	22.1153	25.0134	39.8036
Abs. relative error (%)	0.01	0.12	0.78
$\sqrt{\bar{\lambda}_3}$	61.7890	65.8577	89.0403
$\sqrt{\bar{\lambda}_3}^{[17]}$	61.8069	65.8681	89.3193
Abs. relative error (%)	0.03	0.02	0.31

4. Numerical results for an inward-oriented uniform cantilever beam carrying partially distributed mass attached to a rotating rigid ring

The problem defined in Section 2 (Eq. (2.4) and (2.5)) was solved using the numerical method explained in Section 3 to obtain the dimensionless eigenfrequencies. The location and the amount of partially distributed mass on the rotating beam were investigated. The numerical simulations were performed for dimensionless distributed mass parameter of $\alpha_\mu = 0.5, 1.0$, and 1.5 and the

list of the locations L_1, L_2, and L_3 is given in Table 2. The partially distributed mass having a relative length of 0.5 was located towards the beginning (clamped end), middle, and free end of the beam. These cases are referred to as cases C, M, and F, respectively. The first three dimensionless eigenfrequencies $\bar{\omega_i} = \sqrt{\lambda_i/\lambda_i^{non}}$ $(i = 1, 2, 3)$ of the beam were calculated as a function of dimensionless rotational speed η_i where λ_i^{non} is the i_{th} dimensionless eigenfrequency of the non-rotating beam.

Table 2. The tested positions of the partially distributed mass.

	L_1/L	L_2/L	L_3/L
Case C	0.0	0.5	0.5
Case M	0.25	0.5	0.25
Case F	0.5	0.5	0.0

The validation of the dynamic model and the numerical method was performed by comparing the results with the finite element solution. The finite element model was created using COMSOL 5.4 software. The modulus of elasticity and density was set to 210 GPa and 7850 kg/m^3, respectively. A mesh sensitivity analysis was performed and 100 beam elements were used to model a 100 mm long beam. The case F with $\alpha = 0.5$ was selected for the comparison study. The dimensionless eigenfrequency with respect to dimensionless rotational speed obtained from FEM and the proposed model is shown in Fig. 3. Excellent agreement between the results was obtained. However, the eigenfrequencies at

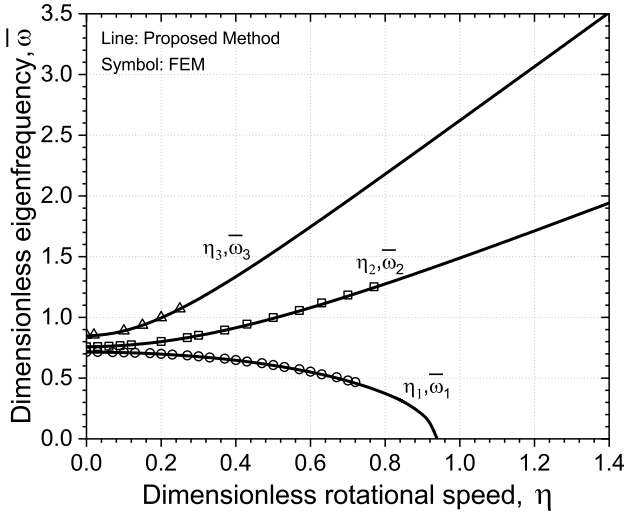

FIG. 3. Comparison of dimensionless eigenfrequency and rotational speed of the inward-oriented uniform cantilever beam attached to a rotating rigid ring ($\alpha = 0.5$, Case F).

some rotational speeds, especially relatively high speeds, could not be obtained using the FEM model due to the lack of a convergent stationary analysis.

Once the comparison study was completed, the proposed model was used to investigate the effect of the location and amount of the distributed mass on the eigenfrequency behavior. The numerical analysis was first performed for $\alpha = 0.5$ and the results are shown in Fig. 4. The analytical results of [17] are also shown as $\alpha_\mu = 0$ for comparison. It can be observed in Fig. 4 that the first three eigenfrequencies of the rotating beam system at a constant rotational speed decreased with increasing partially distributed mass for cases C and M. This behavior was also observed with the first eigenfrequency of Case F. However, the second and third eigenfrequencies of Case F had different characteristics and as the rotational speed increased, the increase on the eigenfrequencies was higher with increasing partially distributed mass. Thus, at a certain rotational speed, the eigenfrequencies were the same regardless of the amount of partially dis-

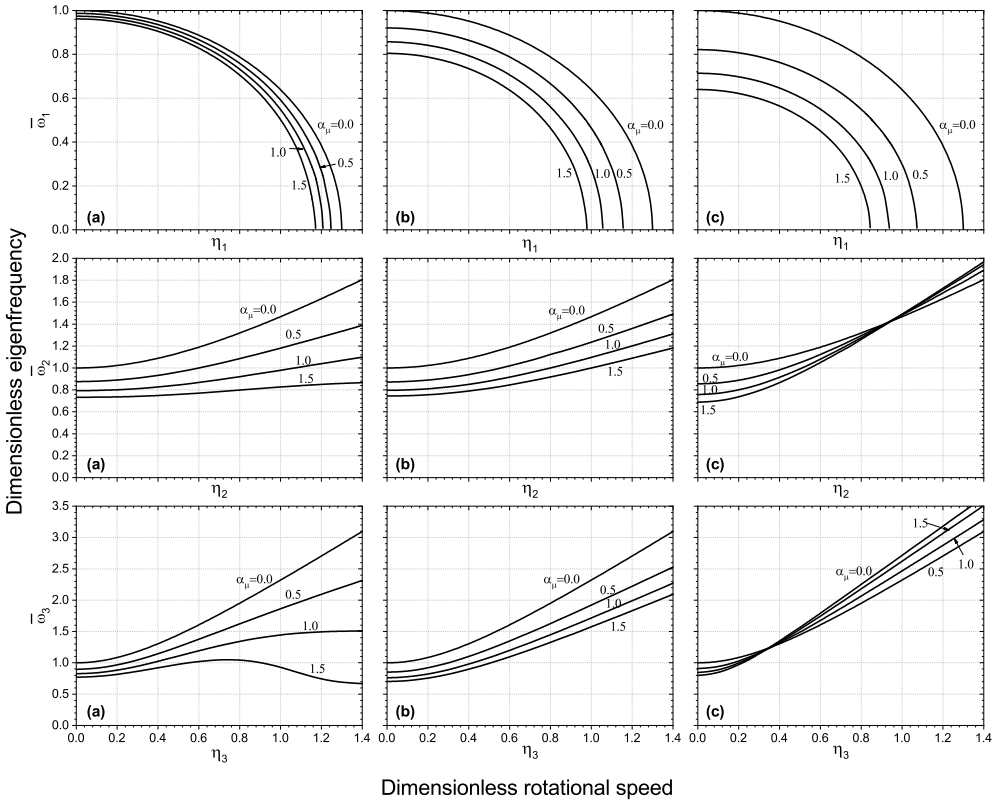

FIG. 4. The variation of the dimensionless eigenfrequency with respect to rotational speed ($\alpha = 0.5$) when $\alpha_\mu = 0.5, 1.0$, and 1.5 is located towards the a) clamped end of the beam (Case C), b) middle of the beam (Case M), and c) free end of the beam (Case F).

tributed mass as shown in Fig. 4(c). Once the rotational speed increased beyond this speed, contrary to the other cases, increasing the partially distributed mass resulted in an increase in the eigenfrequencies.

The results for Case C also indicated that the behavior of the eigenfrequency curves was not always monotonic and the amount of the partially distributed mass affected the eigenfrequency behavior. The curve showed an increase followed by a decrease for $\alpha_\mu = 1.5$ for the third eigenfrequency. A similar behavior was also observed for the second eigenfrequency as the dimensionless distributed mass parameter increased beyond 1.8 ($\alpha_\mu > 1.8$) which was not shown in Fig. 4. However, the descent in the curve was not as steep as observed for the third eigenfrequency. Thus, the effect of rotational speed on the second eigenfrequency can be minimized. For instance, the second dimensionless eigenfrequency for $\alpha_\mu = 1.8$ was between 0.70 and 0.75 within the investigated dimensionless rotational speed range.

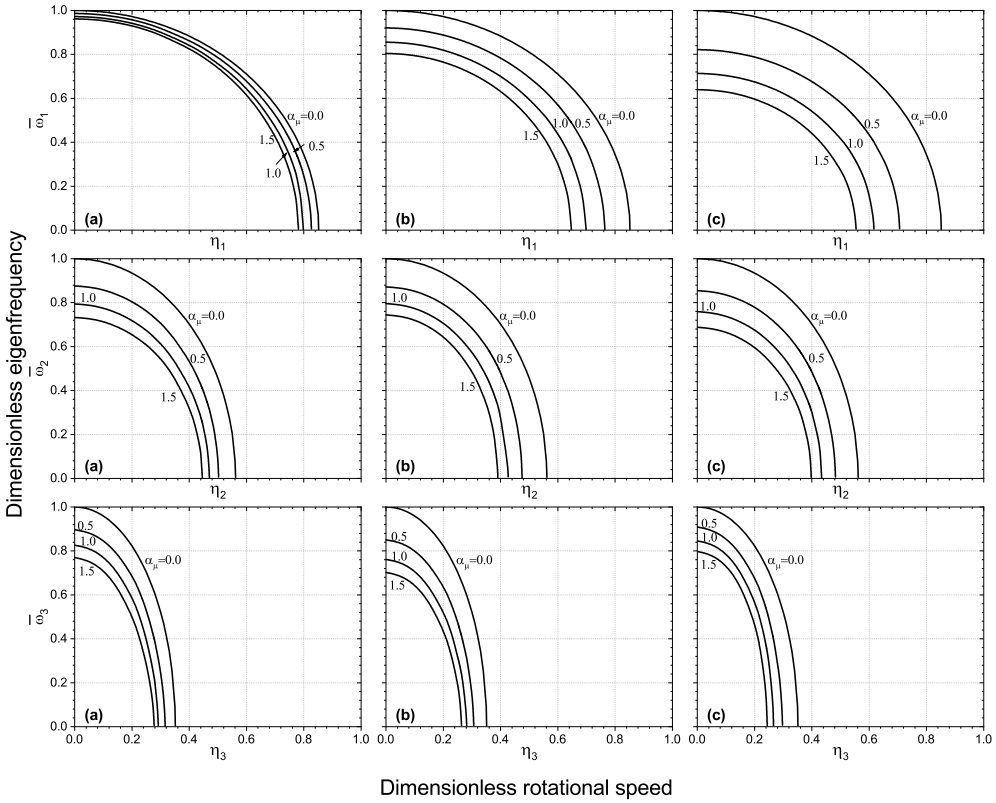

FIG. 5. The variation of the dimensionless eigenfrequency with respect to rotational speed ($\alpha = 1.0$) when $\alpha_\mu = 0.5, 1.0$, and 1.5 is located towards the a) clamped end of the beam (Case C), b) middle of the beam (Case M), and c) free end of the beam (Case F).

A similar analysis was also performed for $\alpha = 1.0$ and $\alpha = 1.5$ and the results are shown in Figs. 5 and 6, respectively. The first eigenfrequency behavior was similar for $\alpha = 0.5, 1.0$ and 1.5 as the dimensionless distributed mass parameter α_μ was increased and the location of the partially distributed mass was changed. However, the second and third eigenfrequencies showed different characteristics compared to $\alpha = 0.5$ and they decreased with increasing rotational speed. Only a slight difference on the second and third eigenfrequencies was observed for a particular α_μ when the location of the partially distributed mass changed. Other observations included the eigenfrequencies at a particular rotational speed decreased with increasing α for all configurations and placing the partially distributed mass at the free end of the beam resulted in a higher decrease on the eigenfrequencies compared to the other locations.

The effect of the partially distributed mass location on the first eigenfrequency was more evident compared to second and third eigenfrequencies. Once

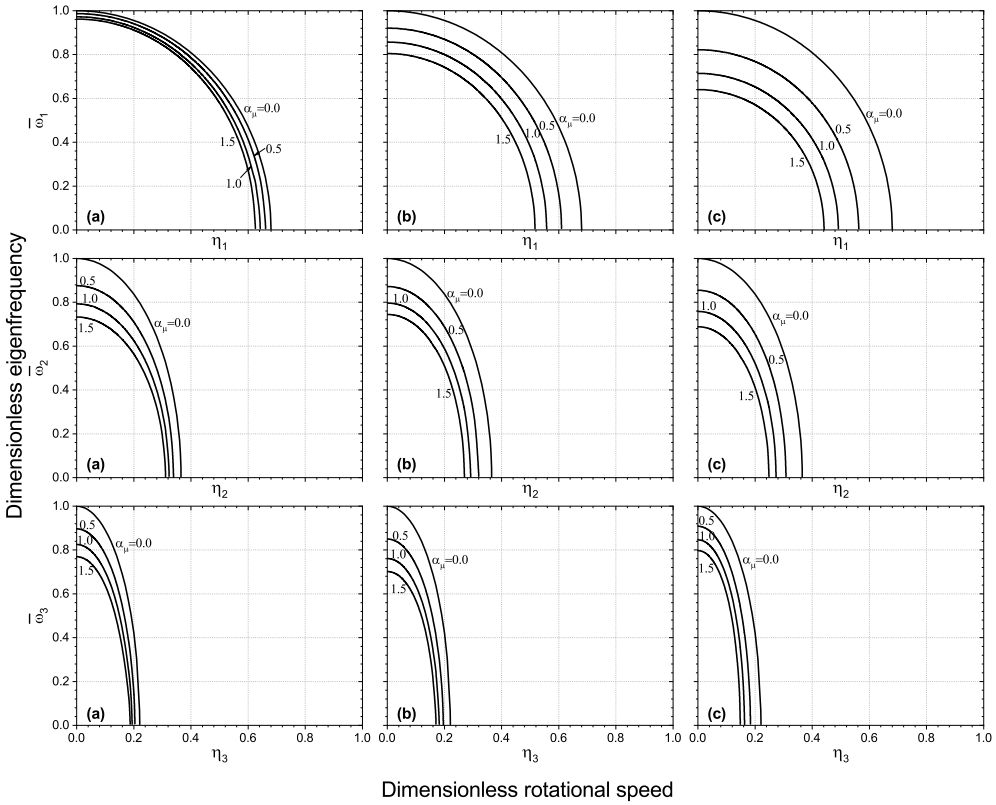

FIG. 6. The variation of the dimensionless eigenfrequency with respect to rotational speed ($\alpha = 1.5$) when $\alpha_\mu = 0.5, 1.0$, and 1.5 is located towards the a) clamped end of the beam (Case C), b) middle of the beam (Case M), and c) free end of the beam (Case F).

the mass moved towards the free end of the rotating beam, the eigenfrequencies had a tendency to decrease, particularly the first eigenfrequency. The amount of partially distributed mass had an inverse effect on the eigenfrequencies. This effect was more apparent in the second and third eigenfrequencies at zero and relatively slow rotational speeds.

The rotational speed at which the eigenfrequencies are zero determines the buckling mode. As shown in Figs. 4–6, only one buckling mode existed for $\alpha = 0.5$ whereas there were three distinguished buckling modes for $\alpha = 1.0$ and $\alpha = 1.5$. An increase in the partially distributed mass decreased the rotational speed at which the buckling would occur. This decrease in the critical rotational speed became smaller with increasing α. The critical rotational speed for buckling was also decreased as the location of the partially distributed mass moved towards the free end of the beam.

5. Conclusions

The differential equation of motion governing the behavior of an inward-oriented uniform cantilever beam carrying an extra partially distributed mass attached to a rotating rigid ring was derived. The Multiquadric (MQ) Radial Basis Functions (RBF) method was used to determine the eigenfrequencies of the beam system. It was observed from the results that as the amount of partially distributed mass increased, the dimensionless eigenfrequency at a constant rotational speed mostly decreased. This behavior could be altered when the partially distributed mass was located towards the free end of the beam for $\alpha = 0.5$. This suggested that a shared dimensionless eigenfrequency existed at a specific rotational speed regardless of the amount of the mass. The monotonic behavior of the eigenfrequency curve also changed when the partially distributed mass was located towards the middle and free end of the beam. This transition was smoother for the second eigenfrequency. Thus, a dimensionless distributed mass parameter α_μ that resulted in essentially constant dimensionless eigenfrequency may be obtained for a wide range of rotational speeds. The location of the partially distributed mass affected the first eigenfrequency more than the second and third eigenfrequencies for $\alpha = 1.0$ and 1.5. One and three rotational speeds for buckling were observed for $\alpha = 0.5$ and $\alpha = 1.0, 1.5$, respectively. An increase in the partially distributed mass decreased the critical rotational speed for buckling. The formulation derived in this study is a first step for further analysis in higher dimensions and the results are expected to improve the practical applications of rotating systems. The proposed numerical model can also be used for other rotating beam problems for which the differential equation of motion is available.

References

1. M.J. Schilhansl, *Bending frequency of a rotating cantilever beam,* Journal of Applied Mechanics, **25**, 28–30, 1958.
2. A.D. Wright, C.E. Smith, R.W. Thresher, J.L.C. Wang, *Vibration modes of centrifugaily stiffened beams*, Journal of Applied Mechanics,Transactions ASME, **49**, 197–202, 1982.
3. T. Yokoyama, *Free vibration characteristics of rotating Timoshenko beams*, International Journal of Mechanical Sciences, **30**, 743–755, 1988.
4. S.V. Hoa, *Vibration of a rotating beam with tip mass*, Journal of Sound and Vibration, **67**, 369–381, 1979.
5. Y.H. Kuo, T.H. Wu, S.Y. Lee, *Bending vibrations of a rotating non-uniform beam with tip mass and an elastically restrained root*, Computers & Structures, **42**, 229–236, 1992.
6. J.S. Rao, W. Carnegie, *Non-Linear Vibrations of Rotating Cantilever Beams*, Aeronautical Journal, **74**, 161–165, 1970.
7. J.S. Rao, W. Carnegie, *Non-linear vibration of rotating cantilever blades treated by the Ritz averaging process,* Aeronautical Journal, **76**, 566–569, 1972.
8. M.N. Hamdan, B.O. Al-Bedoor, *Non-linear free vibrations of a rotating flexible arm*, Journal of Sound and Vibration, **242**, 839–853, 2001.
9. Ö. Turhan, G. Bulut, *On nonlinear vibrations of a rotating beam*, Journal of Sound and Vibration, **322**, 314–335, 2009.
10. E. Pesheck, C. Pierre, S.W. Shaw, *Modal reduction of a nonlinear rotating beam through nonlinear normal modes*, Journal of Vibration and Acoustics Transactions of the ASME, **124**, 229–236, 2002.
11. J. Chung, H.H. Yoo, *Dynamic analysis of a rotating cantilever beam by using the finite element method*, Journal of Sound and Vibration, **249**, 147–164, 2002.
12. N. Mostaghel, I. Tadjbakhsh, *Buckling of rotating rods and plates,* International Journal of Mechanical Sciences, **15**, 429–434, 1973.
13. W.D. Lakin, A. Nachman, *Unstable vibrations and buckling of rotating flexible rods*, Quarterly of Applied Mathematics, **35**, 479–493, 1978.
14. J.T.S. Wang, *On the buckling of rotating rods*, International Journal of Mechanical Sciences, **18**, 407–411, 1976.
15. W.F. White, R.G. Kvaternik, K.R.V. Kaza, *Buckling of rotating beams*, International Journal of Mechanical Sciences, **21**, 739–745, 1979.
16. D.A. Peters, D.H. Hodges, *In-plane vibration and buckling of a rotating beam clamped off the axis of rotation,* Journal of Applied Mechanics,Transactions ASME, **47**, 398–402, 1980.
17. M. Gürgöze, *On the dynamical behaviour of a rotating beam*, Journal of Sound and Vibration, **143**, 356–363, 1990.
18. P. Gross, M. Gürgöze, W. Kliem, *Bifurcation and stability analysis of a rotating beam*, Quarterly of Applied Mathematics, **51**, 701–711, 1993.

19. M. BRØNS, W. KLIEM, *Nonlinear analysis of the buckling and vibration of a rotating elasticum*, International Journal of Mechanical Sciences, **36**, 673–681, 1994.

20. J.B. GUNDA, R.K. GUPTA, R. GANGULI, *Hybrid stiff-string-polynomial basis functions for vibration analysis of high speed rotating beams*, Computer & Structuers, **87**, 254–265, 2009.

21. D. SUSHMA, R. GANGULI, *A collocation approach for finite element basis functions for Euler-Bernoulli beams undergoing rotation and transverse bending vibration*, International Journal of Computational Methods in Engineering Science and Mechanics, **13**, 290–307, 2012.

22. K. SARKAR, R. GANGULI, *Modal tailoring and closed-form solutions for rotating non-uniform Euler-Bernoulli beams*, International Journal of Mechanical Sciences, **88**, 208–220, 2014.

23. V. PANCHORE, R. GANGULI, S.N. OMKAR, *Meshless Local Petrov–Galerkin Method for Rotating Euler-Bernoulli Beam*, Computer Modeling in Engineering and Sciences, **104**, 353–373, 2015.

24. V. PANCHORE, R. GANGULI, S.N. OMKAR, *Meshless local Petrov–Galerkin method for rotating Timoshenko beam: a locking-free shape function formulation*, Computer Modeling in Engineering and Sciences, **108**, 215–237, 2015.

25. M. BERZERI, A.A. SHABANA, *Study of the centrifugal stiffening effect using the finite element absolute nodal coordinate formulation*, Multibody System Dynamics, **7**, 357–387, 2002.

26. E.J. KANSA, Y.C. HON, *A scattered data approximation scheme with applications to computational fluid dynamics: II. Solutions to parabolic, hyperbolic and elliptic partial differential equations*, Computers & Mathematics with Applications, **19**, 147–161, 1990.

27. E.J. KANSA, *Multiquadrics – A scattered data approximation scheme with applications to computational fluid-dynamics-I surface approximations and partial derivative estimates,* Computers & Mathematics with Applications, **19**, 127–145, 1990.

28. B. FORNBERG, T.A. DRISCOLL, G. WRIGHT, R. CHARLES, *Observations on the behavior of radial basis function approximations near boundaries*, Computers & Mathematics with Applications, **43**, 473–490, 2002.

29. A.I. FEDOSEYEV, M.J. FRIEDMAN, E.J. KANSA, *Improved multiquadric method for elliptic partial differential equations via PDE collocation on the boundary*, Computers & Mathematics with Applications, **43**, 439–455, 2002.

30. E. LARSSON, B. FORNBERG, *A numerical study of some radial basis function based solution methods for elliptic PDEs,* Computers & Mathematics with Applications, **46**, 891–902, 2003.

31. G.E. FASSHAUER, *Meshfree Approximation Methods with MATLAB*. World Scientific, New Jersey, 2007.

Received March 8, 2020; revised version June 6, 2020.
Published online August 10, 2020.